Heteroepitaxial barium-doped NaTaO3 films on SrTiO3(001) substrate

Fujiwara, Tomoya ; An, Longjie ; Park, Yohan ; Happo, Naohisa ; Hayashi, Kouichi ; Onishi, Hiroshi

(Citation)
Thin Solid Films,658:66-72

(Issue Date)
2018-07-31

(Resource Type)
journal article

(Version)
Accepted Manuscript

(URL)
https://hdl.handle.net/20.500.14094/90004908

Heteroepitaxial barium-doped $NaTaO_3$ films on $SrTiO_3$(001) substrate

Tomoya Fujiwara[1], Longjie An[1], Yohan Park[1†], Naohisa Happo[2], Kouichi Hayashi[3], Hiroshi Onishi[1*]

[1]Department of Chemistry, School of Science, Kobe University, Rokko-dai, Nada, Kobe, 657-8501 Japan

[2]Graduate School of Information Sciences, Hiroshima City University, Hiroshima, 731-3194 Japan

[3]Department of Physical Science and Engineering, Nagoya Institute of Technology, Gokiso, Showa, Nagoya, 466-8555 Japan

[*]corresponding author: Hiroshi Onishi, Dr., e-mail: oni@kobe-u.ac.jp, phone: +81-78-803-5657

[†]present address: Center for Energy and Environmental Science, Shinshu University, Wakasato, Nagano, 380-8553 Japan

Abstract

Perovskite-structured $NaTaO_3$ films were epitaxially deposited on centimeter-sized $SrTiO_3$(001) wafers by hydrothermal and solvothermal reactions to examine the surface science for an efficient photocatalytic water-splitting reaction. The addition of Ba cations in the starting solutions afforded Ba-doped $NaTaO_3$ films. X-ray fluorescence holography was employed to investigate and confirm the heteroepitaxial relationship between the Ba-doped film and substrate.

- Hydrothermal and solvothermal preparation of $NaTaO_3$ heteroepitaxial films on $SrTiO_3$(001).
- Doping with Ba^{2+} cations up to 4 mol% relative to Ta.
- Feasibility of X-ray fluorescence holography for $NaTaO_3$ film characterization.

1 Introduction

The photocatalytic splitting reaction of water demonstrates promise for the production of hydrogen fuel. Polycrystalline particles of sodium tantalate ($NaTaO_3$) doped with alkaline-earth metal (e.g., Ba, Sr, or Ca) cations exhibit high quantum efficiencies for this reaction [1-4] and also the steam reforming reaction of methane [5] when the bandgap is excited by ultraviolet light. The photocatalytic reduction of CO_2 using pristine [6], metal-doped $NaTaO_3$ [7,8] and also $KTaO_3$ [9] has been reported. Steady-state [10] and time-resolved [11] infrared absorption studies revealed that the recombination of photoexcited electrons and holes is restricted by the doping of alkaline-earth metals into $NaTaO_3$. The restricted recombination in the bulk provides an explanation for the observed increase in the quantum efficiency. In addition, the photoexcited electrons and holes efficiently drive redox reactions at the surface to produce hydrogen and oxygen. Therefore, surface reaction centers on $NaTaO_3$ should be investigated for further development. A series of well-defined, crystalline $NaTaO_3$ films, either doped or undoped with foreign metal cations, are required for surface science studies. In this study, Ba-doped and undoped $NaTaO_3$ films were epitaxially grown on centimeter-sized $SrTiO_3$(001) substrates to satisfy this requirement.

2 Previously reported $NaTaO_3$ films

Thus far, polycrystalline $NaTaO_3$ films have been prepared by hydrothermal reactions [12-15], synthesis under $NaNO_3$ flux [16, 17], and magnetron sputtering [18]. In this study, hydrothermal and solvothermal reactions were employed to produce epitaxial films on $SrTiO_3$ substrates. Typically, hydrothermal [19-25] and solvothermal [26, 27] reactions have been utilized to produce micrometer-sized undoped $NaTaO_3$ particles. In addition, $NaTaO_3$ particles doped with Ca, Sr, and Ba [10], La [28, 29], Bi [30, 31], V [32], or Cu [33] cations were synthesized under hydrothermal reaction conditions. Cubic particles with smooth facets have been reported previously, indicative of the stability of the (001) truncation of a perovskite-structured $NaTaO_3$ lattice in the solutions.

The (001)-oriented $SrTiO_3$ wafers can serve as a good template for the heteroepitaxial growth of oriented $NaTaO_3$ films. $NaTaO_3$ exhibits a perovskite structure that is slightly distorted in orthorhombic symmetry (*Pbnm*, a = 0.548, b = 0.552, c = 0.779 nm) at room temperature [34] and an orthorhombic cell contains four $NaTaO_3$ units. A cube of with sides of 0.389 nm, the volume of which corresponds to one fourth of the orthorhombic cell volume, is effectively assigned to one unit. As $SrTiO_3$ exhibits a perfectly cubic structure with a = 0.390 nm [35], the heteroepitaxial growth of $NaTaO_3$ is expected on $SrTiO_3$ with a small mismatch of the two cubic cells by 0.3%. Indeed, $KTaO_3$ [36–38] with a cubic cell with sides of 0.399 nm [39] and $KNbO_3$ [38, 40] have been reported to be present on the heteroepitaxial films on a $SrTiO_3$(001) substrate under hydrothermal reaction conditions.

In the present study, the authors assume $NaTaO_3$ to be in a pseudo-cubic structure with a = 0.389

nm as illustrated in Fig. 1. They recognize that the real-cubic $NaTaO_3$ appears at temperatures higher than 890 K with a = 0.393 nm [17]. However, identifying and controlling the orientation of the orthorhombic cell is beyond their purpose here. Suzuki *et al*. [17] recently determined a relation of (10-1)[010]$NaTaO_3$//(100)[010]$SrTiO_3$ with orthorhombic $NaTaO_3$ films prepared on $SrTiO_3$(100) through a flux coating method.

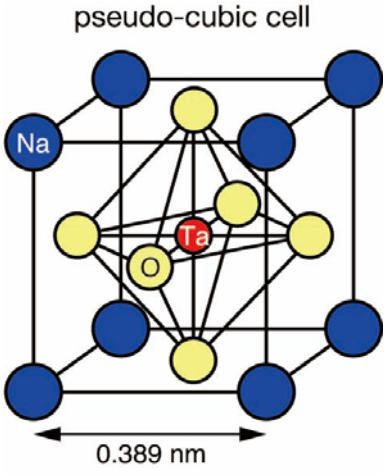

Fig. 1. A pseudo-cubic unit cell of $NaTaO_3$. (Print in a gray scale.)

3 Materials and methods

For hydrothermal synthesis, 15 mol L^{-1} aqueous solutions of NaOH (96%, Wako) containing Ta_2O_5 (99.99%, Rare Metallic Co.) and $BaCO_3$ (99.99%, Wako) were sealed in a Teflon container and heated at 473 K in an autoclave (OMlab-Tech, MR28) for 12 or 24 h. Previously, high concentrations of KOH have been reported to be favorable for $KTaO_3$ production instead of pyrochlore-structured $KTa_2O_5(OH)$ [36]. The solutions exhibited a Na/Ta molar ratio of 30 with Ba/Ta ratios of 0, 0.02, or 0.05. A one-side polished $SrTiO_3$(001) wafer of a square with sides of 10 mm and thickness of 0.5 mm (Shinko-sha) was placed on a Teflon holder in a container (Fig. 2). The polished wafer face was faced downwards, in contact with the solution, to avoid the falling solid particles that precipitated in the solution. The film-covered substrates were rinsed with water and dried in air at 343 K.

In solvothermal synthesis, a 2 mol L^{-1} ethanol solution of $Ta(OC_2H_5)_5$ (99.98% trace metal basis, Sigma-Aldrich) and a 0.2 mol L^{-1} ethanol solution of $Ba(OC_2H_5)_2$ (99%, Kojundo Chemical Laboratory) were mixed in a molar ratio of $Ta(OC_2H_5)_5$:$Ba(OC_2H_5)_2$ = 50:1 and then put in a 15 mol L^{-1} aqueous NaOH solution at 273 K to achieve a Na/Ta molar ratio of 75. The volume ratio of ethanol/water was 12/100 in the starting solution. The as-prepared solution was placed in the autoclave with a $SrTiO_3$ wafer on the holder and heated at 473 K for 12 h.

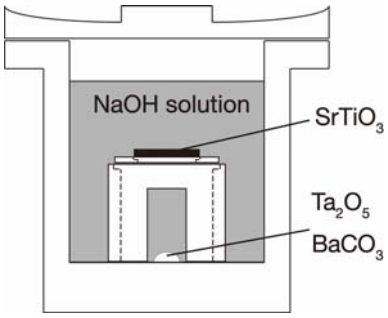

Fig. 2. A $SrTiO_3$(001) wafer in the Teflon container. (Print in a gray scale.)

X-ray photoelectron spectroscopy (XPS) was employed to analyze the film composition by using a spectrometer (Ulvac-Phi, PHI X-tool) with an Al-Kα excitation source. X-ray diffraction (XRD, PANalytical, X'Pert Pro MPD) was employed to determine the crystallographic phases in Yeungnam University. Scanning electron microscopy (SEM, JEOL, JSM-5510) was employed to observe the shape and energy dispersive X-ray spectrum of the films. X-ray fluorescence holography (XFH) was utilized to investigate the epitaxial relationship of the Ba-doped film and single-crystalline $SrTiO_3$ substrate. This is a model-free method for determining the three-dimensional structure of the local atomic arrangements around a specific fluorescing element [41]. A hologram of the Ta Lα fluorescent X-ray was observed at beam line 13XU in SPring-8 synchrotron facility.

4 Results and discussion

4.1 Film composition

Fig. 3(A) shows the wide-scan XPS spectra of the substrate and films. In the spectrum (a) of the $SrTiO_3$ substrate, major signals corresponding to Sr, Ti, O, and C were observed, while a weak emission was observed at a binding energy of 500 eV, possibly related to contamination by Na. An undoped $NaTaO_3$ film prepared by the hydrothermal reaction for 24 h (hereafter referred to as HTM-NTO) exhibited signals corresponding to Na, Ta, and O with no sign of contamination other than the presence of carbon in spectrum (b). The absence of $SrTiO_3$-induced emissions revealed that the substrate is completely covered by a film greater than the photoelectron escape depth, 2 nm, at the Sr 3d and Ti 2p levels. Panels (B), (C), and (D) show separate scans for Na 1s, Ta 4f, and O 1s levels, respectively. The binding energy of each spectrum was calibrated relative to the oxygen 1s level at 530.0 eV to compensate for the charging of the X-ray-irradiated semiconductor wafer. The binding energy of the Ta 4f 7/2 peaks was 25.8 eV. This energy is consistent with that of the $NaTaO_3$ particles prepared for the hydrothermal reaction [10], revealing a +5 oxidation state for the Ta cations. Sharp, symmetric peaks were observed in the Na 1s and Ta 4f spectra, indicating the presence of the homogeneous environment for the metal cations in the film. The raw intensity of the two signals was corrected with the photoemission cross sections and photoelectron escape depths to yield a molar ratio of Na:Ta = 38:62. A Na/Ta ratio of 40:60

was separately derived from the EDX spectrum equipped with SEM (SEM-EDS). XPS is more surface-sensitive than SEM-EDS; hence, the similar ratios observed by the two methods revealed a uniform film composition at different depths from the surface. The Na/Ta ratio was less than unity possibly because Na^+ was partially exchanged by protons incorporated into the film during hydrothermal preparation. The inclusion of OH species has been reported for $NaTaO_3$ [10] and $KTaO_3$ [42] particles prepared by a hydrothermal reaction.

By the addition of $BaCO_3$ into the starting solution, Ba-containing materials were deposited on the substrate during the hydrothermal reaction for 12 h. With a Ba concentration of 2 mol% in the solution relative to Ta, a Ba-doped film was obtained (hereafter referred to as HTM-Ba-NTO). Ba-induced XPS signals were observed in the wide-scan spectrum (c) with intact signals for Na, Ta, and O. A broad peak was observed at 780.2 eV in the separately scanned Ba 3d5/2 spectrum (c) shown in panel (E). The cation composition of the film was estimated as Na:Ta:Ba = 40:58:2 from the XPS signal intensities. These numbers are acceptable for a $NaTaO_3$ film doped with Ba compared to the composition of the undoped film prepared in the same manner. The Ba concentration was 4 mol% relative to Ta. According to SEM-EDS results, a Na:Ta ratio of 45:55 and a Ba fraction was below the limit of detection because of the limited film thickness.

With a high Ba concentration in the starting solution, i.e., 5 mol%, an undesired compound was deposited on the substrate. In the wide-scan spectrum (d), the Na 1s emission weakened, while Sr 3d and Ti 2p signals were observed. The composition estimated from the separate-scan spectra shifted to the ratio of Na:Ta:Ba = 5:48:47 away from the desired ratio. A compound other than Ba-doped $NaTaO_3$ should have incompletely covered the substrate. A longer reaction time, i.e., 24 h, was attempted, however, a film with an undesired composition was still obtained.

Finally, the solvothermal reaction for 12 h was examined to produce a Ba-doped film, namely STM-Ba-NTO. In the wide-scan spectrum (e), the signals of Na, Ta, O, and Ba were observed as expected. The carbon 1s intensity was limited although the Ta and Ba sources in the starting solution comprised ethoxide ligands. The film composition deduced from the separate-scan spectra (e) in panels (B), (D), and (E) was Na:Ta:Ba = 47:49:4. These numbers are satisfactory for a Ba-doped $NaTaO_3$ film. The absence of Sr 3d or Ti 2p signals revealed that the substrate is completely covered by the film. The surface energies of $NaTaO_3$ [43] and $SrTiO_3$ [44] were estimated to be 1.6 and 2.5 J m^{-2}, respectively. The smaller energy of $NaTaO_3$ provides a reason for the complete coverage observed for $SrTiO_3$ on the three films, HTM-NTO, HTM-Ba-NTO, and STM-Ba-NTO.

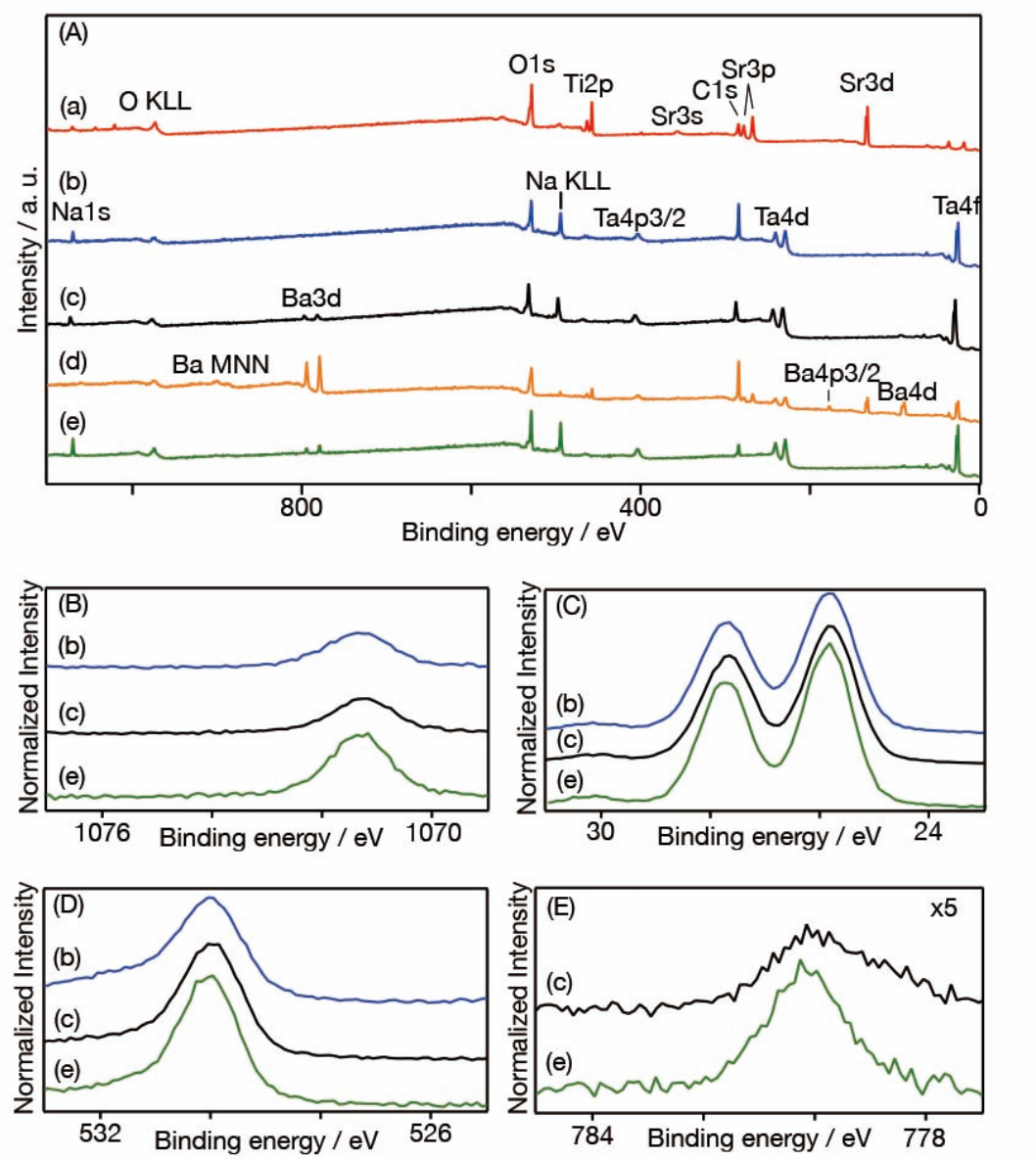

Fig. 3. X-ray photoelectron spectra of the $NaTaO_3$ films on $SrTiO_3$(001). (A) Wide scans in a binding energy range of 0–1100 eV. Separate scans for (B) Na 1s, (C) Ta 4f, (D) O 1s, and (E) Ba 3d5/2 emissions. Spectra of the (a) $SrTiO_3$ substrate, (b) HTM-NTO, (c) HTM-Ba-NTO, (d) the hydrothermally prepared film with a Ba concentration of 5 mol%, and (e) STM-Ba-NTO. The intensity of the separate spectra was normalized relative to that of the O 1s emission. (Print in a gray scale.)

4.2 Crystal structure

The XRD results confirmed the presence of crystallized $NaTaO_3$ films on the substrate. The diffraction pattern (a) in Fig. 4(A) was observed for the naked substrate. Diffraction peaks indexed to (001), (002), and (003) were observed at $2\theta = 23$, 47, and 73°, respectively. Note that the indexes are defined in the pseudo-cubic cell described in Section 2. These peaks were observed in the conventional Bragg–Brentano geometry, where the X-ray source and detector are placed symmetrically relative to the

surface normal of the $SrTiO_3$ wafer. The symmetric geometry was modified by a 1° offset, where $\omega = ½ \times 2\theta +$ offset, for observing the diffraction peaks of the HTM-NTO, HTM-Ba-NTO, and STM-Ba-NTO films. The intense diffraction of the substrate decreased in the asymmetric geometry to recognize diffraction in the films. Three films exhibited peaks at 23° and 47°, corresponding to the (001) and (002) diffractions of $NaTaO_3$, respectively. A diffraction other than a (00n) type was not observed for the films although a number of peaks at 2θ = 40–80° were observed for the $NaTaO_3$ powder. The selected appearance of the (00n) diffraction was related to the crystalline $NaTaO_3$ domains oriented toward the [001] axis parallel to the [001] axis of the substrate.

Attempts were made to further detect the shifts of the (001) peak generated in the films and substrate. The (001) peaks were observed at 22.7 and 22.8° for the substrate and HTM-NTO film, respectively, as shown in panel (B). A positive shift by 0.1° revealed the contraction in the distance of the (001) layer by 0.4%. The contracted distance is in agreement with the lattice sizes described in Section 2. The (001) peak corresponding to HTM-Ba-NTO was observed at 22.7°. Doping with barium led to a shift to a lower angle; thus, the layer distance in the $NaTaO_3$ film increases. Previously [6], Ba^{2+} has been reported to occupy the A sites in the $NaTaO_3$ lattice when doped via the hydrothermal reaction. Assume simple A-site substitution and compare ionic radius of the cations. The layer distance should naturally increase with the substitution of Na^+ with Ba^{2+}. The radii of 12-fold coordinated Na^+ and Ba^{2+} are 0.14 and 0.16 nm, respectively [45]. On the other hand, the lattice spacing can also be sensitive to the fraction of Na^+/proton exchange in the films. When doping with Ba^{2+} decreased Na^+/proton exchange fraction, HTM-Ba-NTO with less protons may have presented a larger spacing than that of HTM-NTO.

In STM-Ba-NTO, the (001) peak shifted back to 22.7°. The reason for this backwards shift is not clear. The lattice spacing can be sensitive to Na^+/proton exchange fraction, as mentioned above. However, the volume ratio of ethanol/water was 12/100 in the solvothermal environment for STM-Ba-NTO film preparation. Since the ratio was far less than unity, the authors expect that the exchange fraction in the films was insensitive to hydrothermal or solvothermal environments.

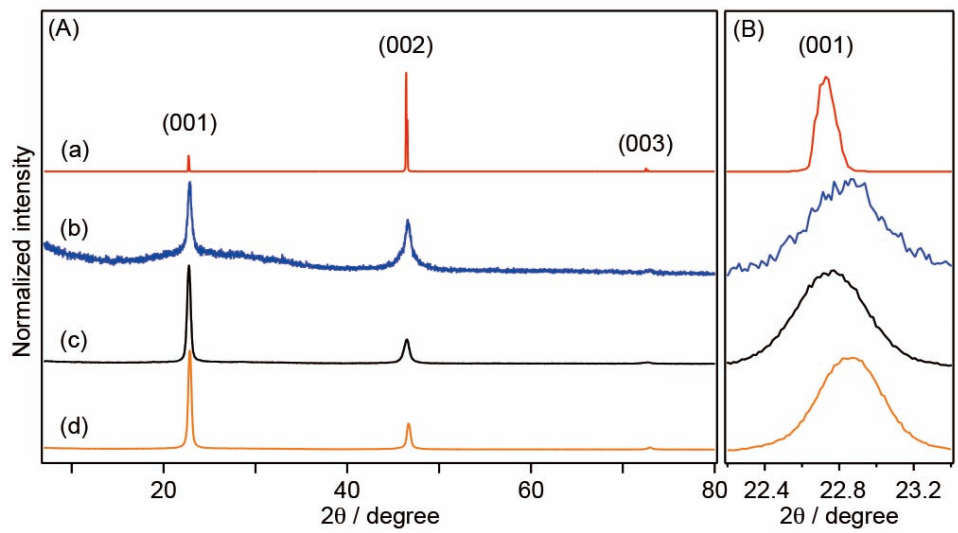

Fig. 4. X-ray diffraction patterns of $NaTaO_3$ films on $SrTiO_3$(001). Peaks observed at 2θ = 7–80° are shown in (A). Shifts of the (001) peak are shown in (B). (a) The $SrTiO_3$ substrate observed in the symmetric geometry. (b) HTM-NTO, (c) HTM-Ba-NTO, and (d) STM-Ba-NTO were observed in the asymmetric geometry. The diffraction intensity was normalized. Peaks with the highest intensity for each pattern are shown with equal heights. (Print in a gray scale.)

4.3 Film morphology

Square-shaped domains were observed in the top-view SEM image of the undoped film HTM-NTO (Fig. 5(A)). Domain boundaries were parallel to the [100] and [010] directions of the $SrTiO_3$(001) substrate. The oriented boundaries suggested an epitaxial relationship between the deposited domains and substrate. The lateral dimension of the domains was greater than or equal to 0.3 μm. The averaged thickness of the film was 0.2 μm according to a cross-sectional SEM image shown in panel (A'). Square-shaped domains were observed with reduced lateral lengths for HTM-Ba-NTO (panel (B)). A cross-sectional image in (B') indicated a reduced thickness of the Ba-doped film.

On the other hand, round-shaped domains partially covering the substrate (panel (C)) were observed for the film prepared by the hydrothermal method with a Ba concentration of 5 mol% in the solution, the composition of which shifted away from the desired Ba-doped $NaTaO_3$. The absence of an epitaxial relationship is natural when the deposited materials are assumed to be different from $NaTaO_3$.

Square-shaped pits were observed for STM-Ba-NTO (panel (D)). The regulated orientation of the pit boundaries suggested an epitaxial relationship between the solvothermally prepared film and substrate. A mosaic-like pseudo epitaxial relationship may also be present, where the in-plane direction of square domains rotates slightly to create low angle domain boundaries.

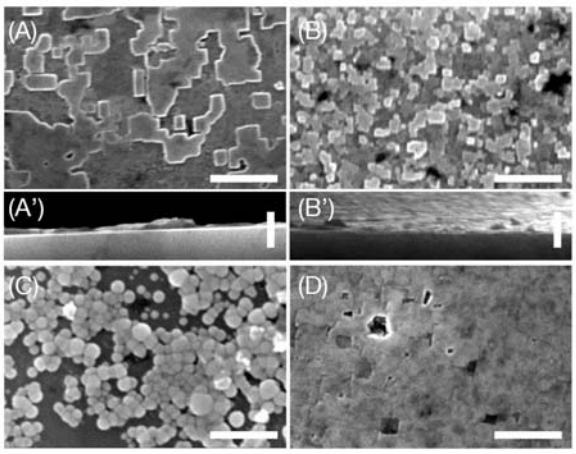

Fig. 5. Scanning electron microscopy images of the $NaTaO_3$ films on $SrTiO_3$(001). Top views of (A) HTM-NTO, (B) HTM-Ba-NTO, (C) the film prepared by a hydrothermal reaction with 5 mol% Ba, and (D) STM-Ba-NTO. Scale bars with a length of 1 μm are inserted in each image. Cross-sectional images of (A') HTM-NTO and (B') HTM-Ba-NTO are shown with 1 μm scale bars. Incident electron energy: 20 keV. (Print in a gray scale.)

4.4 X-ray fluorescence holography

The XPS results described in Subsection 4.1 confirmed the desired composition of the HTM-NTO, HTM-Ba-NTO, and STM-Ba-NTO films comprising undoped and Ba-doped $NaTaO_3$. The XRD results in Subsection 4.2 indicated that the $NaTaO_3$(001) layers are stacked parallel to the surface of the $SrTiO_3$(001) substrate. The square-shaped domains shown in Subsection 4.3 suggested an epitaxial relationship in the lateral directions. In this Subsection, HTM-Ba-NTO was further examined using the holography of Ta Lα fluorescent X-ray to confirm the heteroepitaxial relationship to the substrate.

The principle of holography is briefly described here according to a recent review [41]. The HTM-Ba-NTO film is irradiated by an intense, plane-wave X-ray of wavelength λ (Fig. 6(A)). Atom A adjacent to the fluorescing Ta atom scatters the incident X-ray. The scattered wave superposed on the incident wave affords a standing wave. The Ta atom is excited by the standing wave and emits Lα fluorescent X-ray. The fluorescent X-ray intensity $I(\theta)$ is proportional to the standing wave intensity and is expressed as follows,

$$I(\theta) \;=\; 1 - 2\mathrm{Re}\left(\frac{\lambda r_e f(\alpha)}{2\pi d} e^{2\pi i d(\cos\alpha - 1)/\lambda}\right),$$

with the X-ray scattering factor of A atom $f(\alpha)$, Ta-to-A distance d and the electron radius r_e. Angle α is defined in Fig. 6(A). The amplitude of the second term creating a hologram is often in the order of 10^{-3} relative to the first term giving the background.

In the measurement of HTM-Ba-NTO, $I(\theta)$ was observed using a solid-state detector in a θ range of 0–75° by 1° steps at one azimuth angle, ϕ. Similar θ scans were repeated at different ϕ values of 0–360° in steps of 0.25° to complete one hologram, $I(\theta, \phi)$. Panel (B) shows a Ta Lα hologram thereby

constructed with an incident X-ray of 11.4 keV. The background was subtracted from the raw $I(\theta, \phi)$ to deduce the hologram following an earlier report [46]. X-ray standing wave lines were recognized in the hologram. The presence of the standing wave lines evidenced the epitaxial nature of the Ta-containing film. The three-dimensional distribution of X-ray scattering atoms was reconstructed in an actual space around the Ta atom by the application of the Barton's multiple energy algorithm [47] to the hologram. The hologram was created by interference of the incident and scattered X-rays. Hence the length along *x*, *y* and *z* axes was calibrated by monochromatized X-ray wavelengths.

The two-dimensional distribution on a plane of $z = 0$ was sliced out of the reconstructed three-dimensional distribution and shown in panel (C). The plane of $z = 0$ represented a (001) plane of $NaTaO_3$ involving the fluorescing Ta atom, where the *x* and *y* axes are parallel to the [100] and [010] directions of the $SrTiO_3$ substrate, respectively. Intense and weak scattering was represented by dark and bright colors. Intense scattering was observed at the four corners of the figure. Each scattering at the corners was split into two spots, probably corresponding to the artifacts induced in the reconstruction. The center of the outer spots was assumed to represent the coordinates of the scattering atom. Based on this assumption, four scattering atoms were recognized at $x = \pm 0.39$ and $y = \pm 0.39$ nm, corresponding to the second-nearest Ta atoms placed at (±1, ±1, 0) around the fluorescing Ta atom at (0, 0, 0) in the pseudo-cubic $NaTaO_3$ lattice. The four first-nearest Ta atoms at (1, 0, 0), (-1, 0, 0), (0, 1, 0) and (0, -1, 0) were weakly recognized. The intensity in the reconstructed distributions is proportional to X-ray scattering factor and hence the atomic number of scattering atoms. This relation permits an assumption of the dominant role of Ta over Na or O in the reconstructed distributions. Barium is the other heavy element in the film, but the Ba concentration is not sufficient to contribute the hologram.

A two-dimensional distribution on a plane of $z = 0.39$ nm. Four intense spots were observed on the *x* and *y* axes away from the origin by a distance of 0.39 nm. These spots corresponded to the second-nearest Ta atoms placed at (1, 0, 1), (-1, 0, 1), (0, 1, 1) and (0, -1, 1) in the $NaTaO_3$ film heteroepitaxial to the $SrTiO_3$ substrate. Scattering by the third-nearest Ta atoms at (1, 1, 1) and equivalent positions was not recognized probably due to long distances of fluorescing and scattering atoms. The reconstructed three-dimensional atom distribution was successfully interpreted on the perovskite-structured $NaTaO_3$ lattice; the epitaxial relationship of $NaTaO_3$ deposited on the $SrTiO_3$ substrate is shown.

The authors assume that Ta fluorescence X-ray came from the film, not the underlying substrate. The substrate was Ta free prior to film preparation. If $SrTiO_3$ dissolved and co-precipitated with $NaTaO_3$ in the hydrothermal environment, the substrate might involve Ta atoms. However, the cross-sectional views in Figs. 5(A') and 5(B') presented flat film-substrate interfaces with no sign of $SrTiO_3$ dissolution. Thermal diffusion of Ta atoms from the film into the substrate is not probable at our reaction temperature, 473 K.

The feasibility of XFH for recognizing three-dimensional atomic structures, which was demonstrated in this study by scattering Ta atoms around a fluorescing Ta atom, will further be applied in the determination of the atomic structures around the fluorescing dopant cations of interest, *i.e.* Ba, Sr, or Ca in $NaTaO_3$. Artifacts induced in the reconstruction can decrease via the accumulation of the holograms with different incident X-ray energies and averaging reconstructed distributions [41, 47]. This technique can be applied to neutrons instead of X-ray photons for visualizing light element atoms. A recent development using white neutrons with time-of-flight detection has been reported [48].

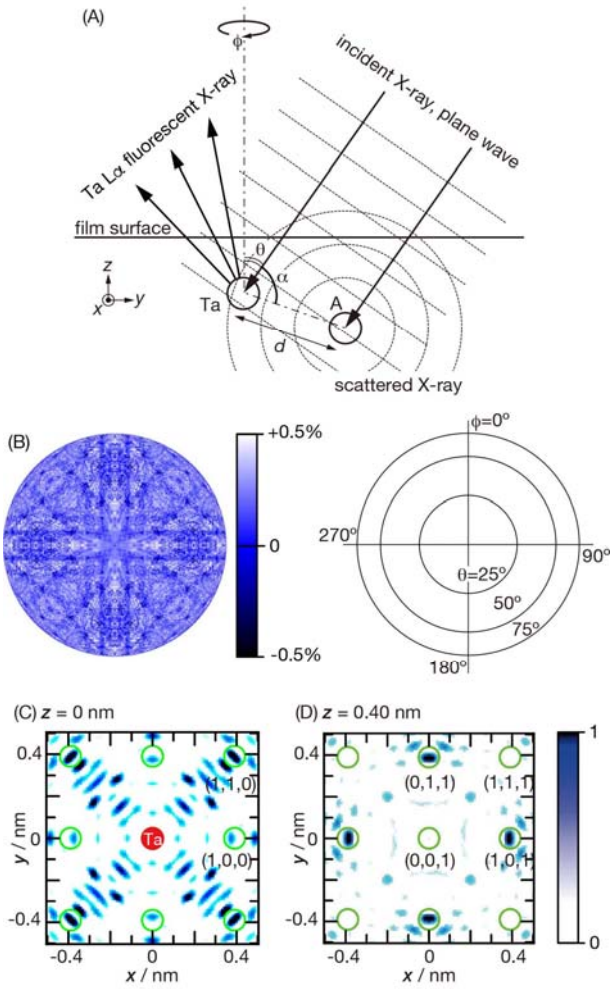

Fig. 6. X-ray fluorescence holography of HTM-Ba-NTO. (A) Definition of angles θ and ϕ. (B) An orthographic projection of the Ta Lα hologram with an incident X-ray energy of 11.4 keV. A scale bar presents hologram amplitude of ±0.5% relative to the background. Reconstructed distribution of scattering atoms on a plane of z = (C) 0 and (D) 0.4 nm. A scale bar shows scattering intensity normalized to 0–1. The fluorescing Ta atom is on the plane of z = 0 and marked in the distribution (C). Eight circles in (C) and nine circles in (D) represent the coordinates of the first-, second-, and third-nearest Ta atoms placed in a crystalline $NaTaO_3$ film heteroepitaxial on the $SrTiO_3$(001) substrate. Atom coordinates are mentioned in the figures. (Print in a gray scale.)

5 Conclusions

Perovskite-structured $NaTaO_3$ films were deposited on centimeter-sized $SrTiO_3$(001) wafers by a hydrothermal or solvothermal reaction. The addition of Ba in the starting solutions afforded Ba-doped $NaTaO_3$ films. The heteroepitaxial relationship of the films and substrates was investigated by XRD and SEM analysis. X-ray fluorescence holography was applied to a Ba-doped film to further provide evidence for the epitaxial relationship suggested by the two other methods.

Acknowledgements

Yoshihiro Ebisu and Takuya Ogura helped the authors in observing X-ray fluorescence holograms. Youngku Sohn of Yeungnam University, Korea afforded facilities for XRD measurements. The X-ray fluorescence measurements were performed at the BL13XU of SPring-8 with the approval of the Japan Synchrotron Radiation Research Institute (Proposal No. 2015B0116, 2016A0116 and 2016B1107). This work was supported by JSPS KAKENHI Grant Number JP15H01046 and JP16H02250.

References

[1] A. Iwase, H. Kato, H. Okutani, A. Kudo, Formation of surface nano-step structures and improvement of photocatalytic activities of $NaTaO_3$ by doping of alkaline earth metal ions, Chem. Lett. 33 (2004) 1260–1261.

[2] A. Kudo, R. Niishiro, A. Iwase, H. Kato, Effects of doping of metal cations on morphology, activity, and visible light response of photocatalysts, Chem. Phys. 339 (2007) 104–110.

[3] A. Iwase, H. Kato, A. Kudo, The effect of alkaline earth metal ion dopants on photocatalytic water splitting by $NaTaO_3$ powder, ChemSusChem 2 (2009) 873–877.

[4] J. Sun, G. Chen, J. Pei, R. Jin, Q. Wang, X. Guang, A simple approach to strontium sodium tantalite mesocrystals with ultra-high photocatalytic properties for water splitting, J. Mater. Chem. 22 (2012) 5609–5614.

[5] K. Shimura, S. Kato, T. Yoshida, H. Itoh, T. Hattori, H. Yoshida, Photocatalytic steam reforming of methane over sodium tantalate, J. Phys. Chem. C 114 (2010) 3493–3503.

[6] K. Teramura, S. Okubo, H. Tsuneoka, T. Shishido, T. Tanaka, Photocatalytic reduction of CO_2 using H_2 as reductant over $ATaO_3$ photocatalysts (A = Li, Na, K), Appl. Catal. B 96 (2010) 565–568.

[7] V. Jeyalakshmi, R. Mahalakshmy, K. R. Krishnamurthy, B. Viswanathan, Photocatalytic reduction of carbon dioxide in alkaline medium on La modified sodium tantalate with different co-catalysts under UV–Visible radiation, Catal. Today 266 (2016) 160–167.

[8] H. Nakanishi, K. Iizuka, T. Takayama, A. Iwase, A. Kudo, Highly active $NaTaO_3$-based photocatalysts for CO_2 reduction to form CO using water as the electron donor, ChemSusChem 10 (2017) 112–118.

[9] K. Li, A. D. Handoko, M. Khraisheh, J. Tang, Photocatalytic reduction of CO_2 and protons using water as an electron donor over potassium tantalate nanoflakes, Nanoscale 6 (2014) 9767–9773.

[10] L. An, H. Onishi, Electron–hole recombination controlled by metal doping sites in $NaTaO_3$ photocatalysts, ACS Catal. 5 (2015) 3196–3206.

[11] M. Maruyama, A. Iwase, H. Kato, A. Kudo, H. Onishi, Time-resolved infrared absorption study of $NaTaO_3$ photocatalysts doped with alkali earth metals, J. Phys. Chem. C 113 (2009) 13918–13923.

[12] Y. Lee, T. Watanabe, T. Takaya, J. N. Kondo, M. Hara, M. Yoshimura, K. Domen, Preparation and characterization of sodium tantalate thin films by hydrothermal−electrochemical synthesis, Chem. Mater. 17 (2005) 2422–2426.

[13] X. Zhou, Y. Chen, H. Mei, Z. Hu, Y. Fan, A facile route for the preparation of morphology-controlled $NaTaO_3$ films, Appl. Surf. Sci. 255 (2008) 2803–2807.

[14] M. Zhang, G. Liu, D. Zhang, Y. Chen, S. Wen, S. Ruan, Facile fabrication of NaTaO3 film and its photoelectric properties, J. Alloy Compound. 602 (2014) 322–325.

[15] L. Polak, T. P. N. Veeken, J. Houtkamp, M. J. Slaman, S. M. Kars, J. H. Rector, R. J. Wijingaarden, Two-step sputter-hydrothermal synthesis of $NaTaO_3$ thin films, Thin Solid Films 603 (2016) 413–417.

[16] S. Suzuki, K. Teshima, K. Yubuta, S. Ito, Y. Moriya, T. Tanaka, T. Shishido, K. Domen, S. Oishi, Direct fabrication and nitridation of a high-quality $NaTaO_3$ crystal layer onto a tantalum substrate, CrystEngComm 14 (2012) 7178–7183.

[17] S. Suzuki, H. Wagata, K. Yubata, S. Oishi, K. Teshima, Epitaxial growth of orthorhombic $NaTaO_3$ crystals on $SrTiO_3$(100) surface by flux coating, CrystEngComm 17 (2015) 9016–9019.

[18] A. Tkach, A. Almeida, J. A. Moreira, J. P. de la Cruz, Y. Romaguera-Barcelay, P. M. Vilarinho, Low-temperature dielectric response of $NaTaO_3$ ceramics and films, Appl. Phys. Lett. 100 (2012) 192909.

[19] Y. He, Y. Zhu, N. Wu, Synthesis of nanosized $NaTaO_3$ in low temperature and its photocatalytic performance, J. Solid State Chem. 177 (2004) 3868–3872.

[20] Y. Lee, T. Watanabe, T. Tanaka, M. Hara, M. Yoshimura, K. Domen, Hydrothermal synthesis of fine $NaTaO_3$ powder as a highly efficient photocatalyst for overall water splitting, Bull. Chem. Soc. Jpn. 80 (2007) 423–428.

[21] J. W. Liu, G. Chen, Z. H. Li, Z. G. Zhang, Hydrothermal synthesis and photocatalytic properties of $ATaO_3$ and $ANbO_3$ (A=Na and K), Int. J. Hydrogen Energy 32 (2007) 2269–2272.

[22] X. Li, J. Zang, Facile hydrothermal synthesis of sodium tantalate ($NaTaO_3$) nanocubes and high photocatalytic properties, J. Phys. Chem. C 113 (2009) 19411–19418.

[23] J. Shi, G. Liu, N. Wang, C. Li, Microwave-assisted hydrothermal synthesis of perovskite $NaTaO_3$ nanocrystals and their photocatalytic properties, J. Mater. Chem. 22 (2012) 18808–18813.

[24] P. Xiong, G. Tan, W. Zhang, A. Xia, H. Ren, Study on photocatalytic activity of $NaTaO_3$ powder synthesized by hydrothermal method, J. Cluster Sci. 24 (2013) 515–522.

[25] Q. Zhang, Z. Li, S. Wang, R. Li, X. Zhang, Z. Liang, H. Han, S. Liao, C. Li, Effect of redox cocatalysts location on photocatalytic overall water splitting over cubic $NaTaO_3$ semiconductor crystals exposed with equivalent facets, ACS Catal. 6 (2016) 2182–2191.

[26] Y. He, Y.Zhu, Solvothermal synthesis of sodium and potassium tantalate perovskite nanocubes, Chem. Lett. 33 (2004) 900–901.

[27] W. Jiang, X. Jiao, D. Chen, Photocatalytic water splitting of surfactant-free fabricated high surface area $NaTaO_3$ nanocrystals, Int. J. Hydrogen Energy 38 (2013) 12739–12746.

[28] X. Li, J. Zang, Hydrothermal synthesis and characterization of lanthanum-doped $NaTaO_3$ with high photocatalytic activity, Catal. Commun. 12 (2011) 1380–1383.

[29] V. Jeyalakshmi, R. Mahalakshmy, K. R. Krishnamurthy, B. Viswanathan, Photocatalytic reduction of carbon dioxide in alkaline medium on La modified sodium tantalate with different co-catalysts under UV–Visible radiation, Catal. Today 266 (2016) 160–167.

[30] X. Wang, H. Bai, Y. Meng, Y. Zhao, C. Tang, Y. Gao, Synthesis and optical properties of Bi^{3+} doped $NaTaO_3$ nano-size photocatalysts, J. Nanosci. Nanotechnol. 10 (2010) 1788–1793.

[31] P. Kanhere, Y. Tang, J. Zheng, Z. Chen, Synthesis, photophysical properties, and photocatalytic applications of Bi doped $NaTaO_3$ and Bi doped $Na_2Ta_2O_6$ nanoparticles, J. Phys. Chem. Solids 74 (2013) 1708–1713.

[32] Y. Gao, Y. Su, Y. Meng, S. Wang, Q. Jia, X. Wang, Preparation and photocatalytic mechanism of vanadium doped $NaTaO_3$ nanoparticles, Integrated Ferroelectrics 127 (2011) 106–115.

[33] Y. Liu, Y. Su, H. Han, X. Wang, Hydrothermal preparation of copper doped $NaTaO_3$ nanoparticles and study on the photocatalytic mechanism J. Nanosci. Nanotechnol. 13 (2013) 853–857.

[34] B. J. Kennedy, A. K. Prodjosantoto, C. J. Howard, Powder neutron diffraction study of the high temperature phase transitions in $NaTaO_3$, J. Phys. Condens. Matter 11 (1999) 6319–6328.

[35] Y. A. Abramov, V. G. Tsirelson, V. E. Zavodnik, S. A. Ivanov, I. D. Brown, The chemical bond and atomic displacements in $SrTiO_3$ from x-ray diffraction analysis, Acta Cryst. B 51 (1995) 942–951.

[36] G. K. L. Goh, C. G. Levi, F. F. Lange, Hydrothermal epitaxy of $KTaO_3$ thin films, J. Mater. Res. 17 (2002) 2852–2858.

[37] H. Hayashi, Y. Hakuta, Hydrothermal epitaxy of $KTaO_3$ thin films under supercritical water conditions, J. Mater. Sci. 43 (2008) 2342–2347.

[38] G. K. L. Goh, K. Y. S. Chan, B. S. K. Tan, Y. W. Zhang, J. H. Kim, T. Osipowicz, Low-temperature epitaxy of $KTaO_3$ and $KNbO_3$ films, J. Electrochem. Soc. 155 (2008) D52–D53.

[39] P. Vousden, A study of the unit-cell dimensions and symmetry of certain ferroelectric compounds of niobium and tantalum at room temperature, Acta Cryst. 4 (1951) 373–376.

[40] A. D. Handoko, G. K. L. Goh, R. X. Chew, Piezoelectrically active hydrothermal $KNbO_3$ thin films, CrystEngComm 14 (2012) 421–427.

[41] K. Hayashi, N. Happo, S. Hosokawa, W. Hu, T. Matsushita, X-ray fluorescence holography, J. Phys. Condens. Matter 24 (2012) 093201.

[42] G. K. L. Goh, S. M. Haile, C. G. Levi, F. F. Lange, Hydrothermal synthesis of perovskite and pyrochlore powders of potassium tantalate, J. Mater. Res. 17 (2002) 3168–3176.

[43] S. K. Sahu, S. Zlotnik, A. Navrotsky, P. M. Vilarinho, Thermodynamic stability of lead-free alkali niobate and tantalate perovskites, J. Mater. Chem. C 3 (2015) 7691–7698.

[44] S. K. Sahu, P. S. Maram, A. Navrotsky, Thermodynamics of nanoscale calcium and strontium titanate perovskites, J. Am. Ceram. Soc. 96 (2013) 3670–3676.

[45] R. D. Shannon, Revised effective ionic radii and systematic studies of interatomic distances in halides and chalcogenides, Acta Cryst. A 32 (1976) 751–767.

[46] N. Happo, K. Hayashi, S. Hosokawa, Data analysis of X-ray fluorescence holography by subtracting normal component from inverse hologram, Jpn. J. Appl. Phys. 49 (2019) 116601.

[47] J. J. Barton, Removing multiple scattering and twin images from holographic images, Phys. Rev. Lett. 67 (1991) 3106–3109.

[48] K. Hayashi, K. Ohoyama, N. Happo, T. Matsushita, S. Hosokawa, M. Harada, Y. Inamura, H. Nitani, T. Shishido, K. Yubata, Multiple-wavelength neutron holography with pulsed neutrons, Sci. Adv. 3 (2017) e1700294 and references therein.